Research Article

Journal of PeptideScience

Received: 2 June 2011 Revised: 15 August 2011 Accepted: 25 August 2011 Published online in Wiley Online Library: 21 November 2011

(wileyonlinelibrary.com) DOI 10.1002/psc.1418

Solid-state NMR reveals differences in the packing arrangements of peptide aggregates derived from the aortic amyloid polypeptide medin

Hannah A. Davies, Jillian Madine and David A. Middleton*

Several polypeptides aggregate into insoluble amyloid fibrils associated with pathologies such as Alzheimer's disease, Parkinson's disease and type 2 diabetes. Understanding the structural and sequential motifs that drive fibrillisation may assist in the discovery and refinement of effective therapies. Here we investigate the effects of three predicted amyloidogenic regions on the structure of aggregates formed by medin, a poorly characterised polypeptide associated with aortic medial amyloidosis. Solid-state NMR is used to compare the dynamics and sheet packing arrangement of the C-terminal region encompassing residues $F^{43}GSV$ within full-length medin ($Med_{1\text{-}50}$) and two shorter peptide fragments, $Med_{30\text{-}50}$ and $Med_{42\text{-}49}$, lacking specific sequences predicted to be amyloidogenic. Results show that all three peptides have different aggregate morphologies, and $Med_{30\text{-}50}$ and $Med_{1\text{-}50}$ have different sheet packing arrangements and dynamics to $Med_{42\text{-}49}$. These results imply that at least two of the three predicted amyloidogenic regions are required for the formation and elongation of medin fibres observed in the disease state. Copyright © 2011 European Peptide Society and John Wiley & Sons, Ltd.

Keywords: aortic medial amyloid; electron microscopy; structure; dynamics

Introduction

Amyloidogenic proteins are recognised by their ability to form fibrils with an affinity for amyloid-specific dyes such as Congo red and thioflavin T [1]. The deposition of these insoluble fibrils is associated with pathologies such as Alzheimer's disease, type 2 diabetes and Parkinson's disease [2]. The characteristic core of fibrils is typically described as a cross-β structure; β-strands are hydrogen bonded approximately perpendicular to the fibril axis with the possibility for side chain groups of separate β-sheet layers to interlock as a steric zipper [3,4]. It is thought that many proteins are able to form amyloid-like fibrils and the quest to find structural and sequential motifs that identify amyloid propensity is ongoing. Studies of short peptide fragments of amyloid-forming proteins can provide insight into the effect of sequence and the role of individual residues on the overall structure of aggregates formed [5,6]. Studies of this kind can identify key stabilising features that can be targeted therapeutically [7].

Advances in high-resolution structural techniques such as solid-state nuclear magnetic resonance (SSNMR) allow these subtle changes in sequence to be investigated at the molecular level. Previous studies of amyloid proteins and fragments thereof have revealed that sequence truncations can lead to substantial changes in the overall morphology of the aggregates formed [8]. For example, fibrils formed by the 40-residue β-amyloid peptide $A\beta_{1\text{-}40}$ comprise parallel and in-register hydrogen bonded β-strands [9–11]. This organisation is reproduced in fibrils of the 26-residue peptide fragment $A\beta_{10\text{–}35}$ [12,13], whereas the shorter peptides $A\beta_{16\text{-}22}$ and $A\beta_{11\text{–}25}$ adopt an antiparallel β-strand arrangement within fibrils, with a pH-dependent registry in the case of $A\beta_{11\text{–}25}$ [14,15].

Aortic medial amyloid is the most common form of localised amyloid and is found in 98% of the White population over the age of 50 [16]. The polypeptide medin, a 50-residue cleavage product of the protein lactadherin, is the principal protein component of plaques found in the aorta and other large arteries in close association to the internal elastic laminae [17]. These plaques are thought to contribute to age-related diminished elasticity of the blood vessels, and experimental evidence suggests that this has a role in sporadic thoracic aneurysm and dissection [18]. The 18–19 C-terminal residues of medin constitute an amyloid-promoting region, and the peptide $Med_{42\text{-}49}$ comprising residues $H_2N\text{-}N^{42}FGSVQFV\text{-}COOH$ of medin is capable of forming highly ordered fibrils within 48 h [19,20].

Our earlier structural studies of needle-like aggregates of $Med_{42\text{-}49}$ using SSNMR and X-ray fibre diffraction revealed β-sheets of hydrogen-bonded peptides in an in-register, parallel configuration. Measurements of $^{13}C\text{-}^{13}C$ dipolar couplings indicated a much closer distance between residues F43 and V46 than is possible within a single β-sheet. We proposed a structural model in which pairs of β-sheets are stabilised by π-π interactions between F43 and F48 of opposing sheet layers [21]. As no structural model is available for full-length medin fibrils, it is not known whether the molecular arrangement within $Med_{42\text{-}49}$ fibres is reproduced in fibrils of full-length medin ($Med_{1\text{-}50}$). Here, SSNMR is used to

* Correspondence to: David A. Middleton, David, University of Liverpool, Crown Street, Liverpool, L69 7ZB, UK. E-mail: middleda@liverpool.ac.uk

Institute of Integrative Biology, University of Liverpool, Crown Street, Liverpool, L69 7ZB, UK

compare the molecular organisation of Med_{42-49} with the organisation of the corresponding region of Med_{1-50} and a 21-residue peptide fragment Med_{30-50}. The aim of this work is to see how the inclusion or omission of different predicted amyloidogenic hot spots affects the structure of the resultant fibrils.

Experimental

Preparation of Fibrils

Synthetic Med_{1-50}, Med_{30-50} and Med_{42-49} were purchased from Peptide Protein Research (Hampshire, UK) Ltd. Each peptide was uniformly ^{13}C and ^{15}N labelled within the sequence FGSV corresponding to residues 43–46. The lyophilised peptides were not fully soluble in aqueous solution and so were initially dissolved in 100% DMSO and then diluted with 10 mM phosphate buffer in ddH_2O, pH 7.4, to a final DMSO concentration of 10% (v/v) and a peptide concentration of 0.25 mM. The solution was incubated at room temperature with agitation for up to 21 days.

Aggregation kinetics

The formation of amyloid was monitored using Thioflavin T (ThT) fluorescence. At each time point (0, 2, 4, 7, 14 and 21 days), 20 µl was removed from the incubated sample and frozen at −20 °C for later analysis. Upon completion of the time course, the samples were defrosted and added to 180 µl of 10 µM ThT in 10 mM Tris, pH 7.5. The mixture was vortexed and transferred to a 1 cm path length cuvette. Measurements were carried out on a Cary Eclipse Varian fluorescence spectrophotometer (Varian, Inc.); enhanced emission at 482 nm following excitation at 450 nm indicates the presence of the characteristic amyloid cross-β structure.

Morphology of medin aggregates

Transmission electron microscopy (TEM) was used to analyse the morphology of the fibrils generated from each peptide. Ten microlitres of fibril solution was loaded onto carbon-coated copper grids and stained with 4% uranyl acetate. The grids were visualised on a Tecnai 10 electron microscope at 100 kV.

Analysis of structure and dynamics by solid-state NMR

Cross-polarisation magic-angle spinning (MAS) ^{13}C SSNMR experiments were performed on hydrated fibrils (5-mg peptide) with a Bruker Avance 400 spectrometer operating at a magnetic field of 9.3 T. Hydrated peptide aggregates were packed by centrifugation into a 4-mm zirconium rotor and rotated at the magic angle at rates between 6 and 13 kHz (±1 Hz). All experiments utilised an initial 4.0-µs ^{1}H 90° excitation pulse length, 1-ms Hartmann-Hahn contact time at a ^{1}H nutation frequency of 65 kHz, two-pulse phase-modulated proton decoupling [22] at a field of 85 kHz during signal acquisition and a 2-s recycle delay.

Two-dimensional ^{13}C-^{13}C broadband dipolar recoupled spectra were obtained using the dipolar assisted rotational resonance (DARR) experiment [23]. Spectra were recorded with 128 hypercomplex points in the indirect dimension (t_1), with a mixing time of 20 ms during which the proton nutation frequency was adjusted to the spinning frequency of 8 kHz. Chemical shift values were referenced to external adamantane at 37.8 ppm. A two-dimensional version of the rotational resonance (RR) exchange experiment [21] was used to selectively observe the dipolar interactions between the aromatic ring (Fϕ) and valine methyl (Vδ/Vδ′) ^{13}C spins. Spectra were recorded with 64 hypercomplex points in the indirect dimension (t_1), and the spinning frequency (ω_R) was adjusted to the difference in the resonance frequencies ($\Delta\Omega_{CC}$) for the Fϕ and Vδ spins (i.e., the $n = 1$ RR condition). Protons were decoupled at 100 kHz during a mixing time of 30 ms.

Site-specific ^{13}C-^{1}H dipolar couplings, which are sensitive to local dynamics on the µs–ms timescale, were measured using the constant time dipolar and chemical shift (CT-DIPSHIFT) correlation experiment [24]. In a series of eight experiments, peak intensities were measured for eight t_1 intervals, where t was incremented from zero to one rotor period ($2\pi/\omega_R$) at a spinning frequency of 6 kHz. The eight spectra (S_n), each defined by 1024 points, were then replicated 16 times and concatenated (S_1, S_2 … S_8, S_1, S_2 … S_8, etc), to give a 1024 × 128 matrix, which was Fourier transformed in the indirect dimension to produce the pseudo–two-dimensional spectra, with the ^{13}C chemical shift information in the

Zyggregator

RLDKQGNF**NA WVAG**SYGND**Q WLQ**VDLGSSK E**VTGII**TQGA RNFG**SVQFVA**

Aggrescan

RLDKQGNF**NA WVA**GSYGNDQ WLQVDLGSSK E**VTGII**TQGA RNF**GSVQFVA**

PASTA

RLDKQGNFNA WVAGSYGNDQ WLQVDLGSSK **EVTGII**TQGA RNFGS**VQFV**A

Figure 1. Aggregation-prone regions of Med_{1-50} as predicted by the three independent methods: Zyggregator, Aggrescan and PASTA. Bold and underlined regions are predicted to contribute to the cross-β core of fibrillar aggregates.

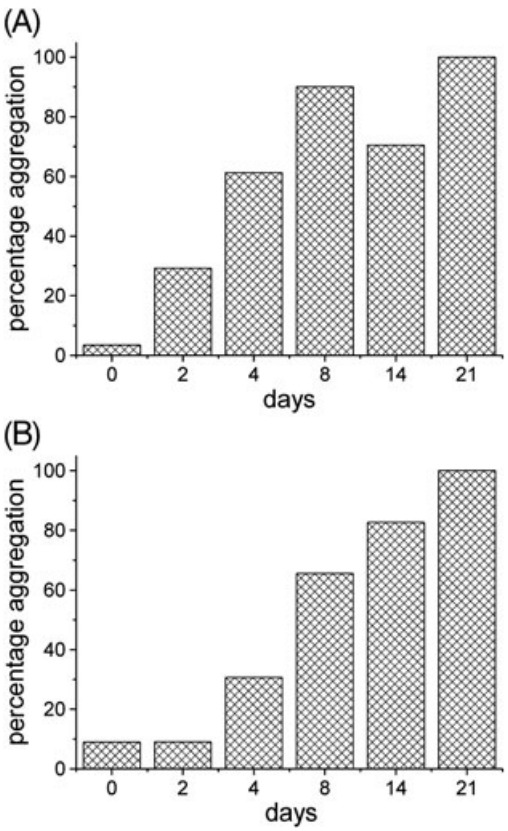

Figure 2. Thioflavin T fluorescence intensity of Med_{30-50} (A) and Med_{1-50} (B) over 21 days. Values are shown as a percentage of intensity values at 21 days.

Journal of PeptideScience

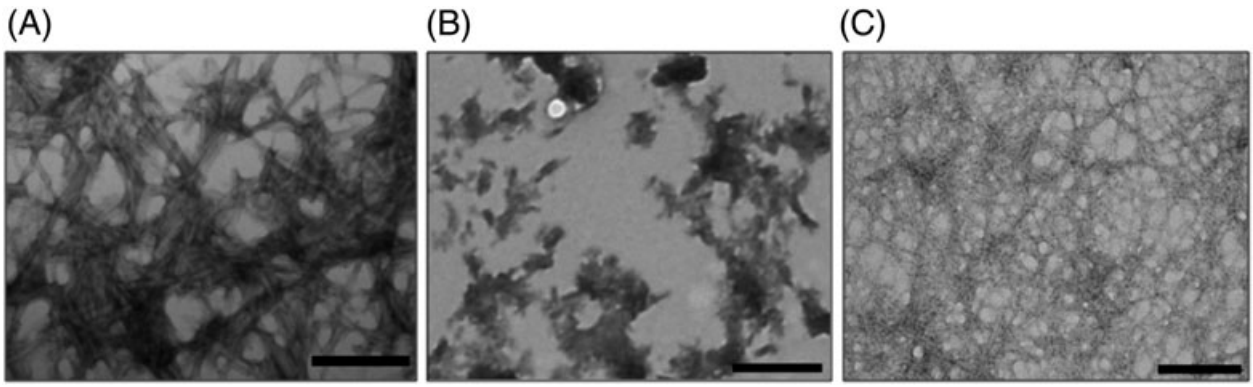

Figure 3. TEM images for Med_{42-49} (A) and Med_{30-50} (B) and Med_{1-50} (C). Scale bars equate to 500 nm (A) and 1000 nm (B and C).

direct dimension and C-H dipolar coupling information in the indirect dimension. Values of the dipolar coupling strength were determined by finding the closest agreement between the observed dipolar spectra and spectra simulated for different values of the dipolar anisotropy [24,25]. DIPSHIFT spectra were recorded, at 4 °C and the lengthier ^{13}C-^{13}C spectra were recorded at −10 °C to minimise sample dehydration. Chemical shifts were identical at the two temperatures.

Results and Discussion

Several computational methods are available for predicting aggregation-prone regions of peptides based on the physico-chemical properties of the constituent amino acids, and these can provide a useful starting point for experimental investigations of amyloidogenic peptides. Analysis of the medin sequence using three predictive methods, Zyggregator, Aggrescan and PASTA [26–28], consistently highlighted the region encompassing residues 46–49 as being prone to aggregation (Figure 1), in agreement with the known amyloidogenicity of the peptide Med_{42-49} [21]. Two of the three methods also predicted that V^{32}TGII and N^{9}AWVA are prone to aggregation (Figure 1). Based on these predictions, the aggregation characteristics of Med_{1-50} and Med_{42-49} were therefore investigated alongside a third peptide Med_{30-52}, which contains the VTGII sequence but not NAWVA.

Earlier *in situ* SSNMR analysis of Med_{42-49} aggregation indicated that large or insoluble species occurred after monitoring for 6 h with aggregation reaching completion by 24 h [21]. Med_{42-49} aggregation is not accompanied by an increase in ThT fluorescence and so could not be studied by this method. ThT insensitivity for short amyloidogenic peptides is often observed [29], although the reasons are not well understood. A general model was proposed in which ThT binds with the long axis of the dye parallel with the long hydrogen-bonding axis shared by all fibrillar assemblies [30], although a recent study on the prion peptide GNNQQNY suggests that ThT adsorbs to the fibrils parallel with the peptide strands (i.e., perpendicular to the fibril axis) [31]. For Med_{42-49}, it is possible that the length of the peptide strand and/or the properties of the exposed residues do not favour ThT binding or fluorescence enhancement. By contrast, Med_{30-50} and Med_{38-50} give rise to the typical increase in ThT fluorescence associated with amyloid formation (Figure 2). Med_{1-50} aggregation is preceded by a lag phase of 2 days consistent with nucleation-dependent growth and fibril growth approaches the ThT end point by 21 days.

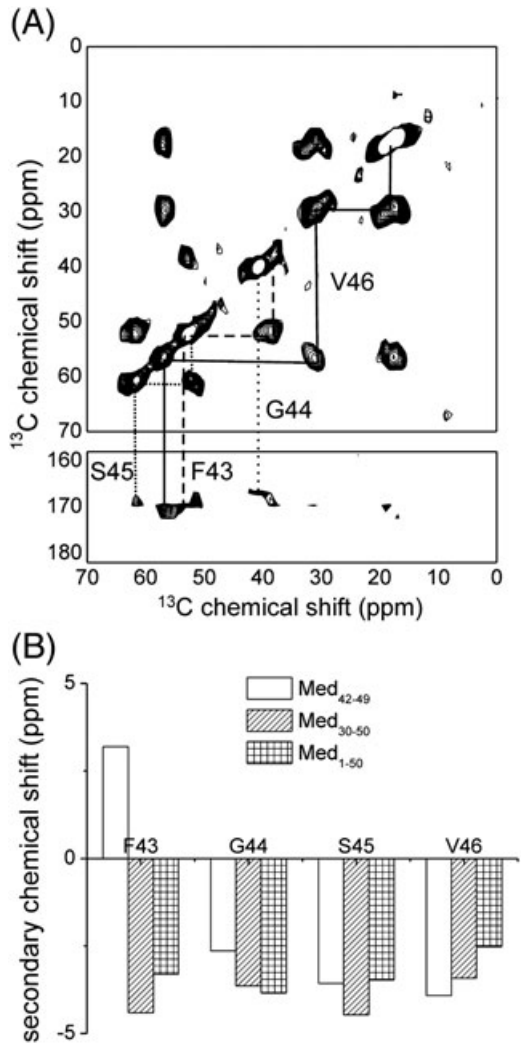

Figure 4. (A) Regions of a representative ^{13}C DARR spectrum for Med_{30-50} with dashed lines showing peak assignments to the F43, G44, S45 and V46 spin systems. ^{13}C chemical shifts for Med_{42-49}, Med_{30-50} and Med_{1-50} are summarised in Table 1. (B) Secondary chemical shifts ($\Delta\delta$) for residues F43, G44, S45 and V46 of Med_{42-49}, Med_{30-50} and Med_{1-50}. Values are calculated as $\Delta\delta = (\delta C\alpha - \delta C\beta)_{RC} - (\delta C\alpha - \delta C\beta)_{obs}$, where $\delta C\alpha$ and $\delta C\beta$ are the chemical shift values for Cα and Cβ, respectively, and subscripts RC and obs denoted the mean random coil [41] and observed values, respectively. Positive values of $\Delta\delta$ are consistent with a helical structure, and negative values are consistent with a β-strand structure.

Med_{30-50} does not show the same lag phase and reaches the end point after 8 days. This indicates that aggregation of the larger peptides is much slower than for Med_{42-49}. TEM analysis of the three peptide aggregates isolated after 2 (Med_{42-49}) or 21 days (Med_{30-50} and Med_{1-50}) reveals striking differences in their morphologies (Figure 3). Med_{42-49} forms rod-like fibres, Med_{1-50} shows a dense network of slender, amyloid-like fibrils and Med_{30-50} aggregates appear to be rather granular in character. Med_{42-49} aggregates isolated after 21 days were not significantly different from the aggregates after 2 days (not presented). Hence, the aggregation kinetics and resulting morphology of the medin-derived peptides are highly sensitive to their length and/or sequence.

The aggregates were examined in further detail using SSNMR to compare the secondary structure and packing arrangement of the C-terminal sequence encompassing residues $F^{43}GSV$, which were labelled with ^{13}C to enhance sensitivity. A representative ^{13}C DARR spectrum of Med_{30-50} is shown in Figure 4A, and the measured chemical shift values for the $F^{43}GSV$ sequence of all three peptide aggregates are given in Table 1. Although the accuracy of the measurements is compromised to some extent by the NMR line widths (typically 1.0–2.0 ppm), the chemical shift values nevertheless show some interesting site-specific and peptide-specific differences. The values for Cα of F43 cover a range of $>$2.5 ppm, and values for Cα and Cβ of G44 and V46 also differ by 1.0–1.5 ppm. This distribution of values for the three peptides may reflect differences in local conformation within the $F^{43}GSV$ sequence. Secondary chemical shift ($\Delta\delta$) values calculated from the Cα and Cβ chemical shift values (Figure 4B) are largely negative, however, and thus broadly consistent with a β-sheet structure across the C-terminal region. F43 of Med_{42-49} is exceptional in giving a positive $\Delta\delta$ value, which is consistent with an α-helical geometry. Unlike for the longer peptides, F43 is close to the N-terminal of Med_{42-49}, and its geometry may therefore be more weakly constrained by neighbouring residues. Interestingly, chemical shift values for the F43 ring are quite similar for Med_{30-50} and Med_{1-50} but somewhat different for Med_{42-49}, implying that the shorter peptide may have a different side chain packing arrangement to the longer peptides.

The side chain packing of F43 in the three peptide aggregates was examined further using selective dipolar recoupling NMR measurements. A two-dimensional exchange spectrum of Med_{42-49} at a MAS rate of 11 126 Hz, which corresponds to $n = 1$ rotational resonance with respect to the Fϕ and Vγ/Vγ' frequencies, shows cross-peaks correlating the ^{13}C-^{13}C dipolar coupling between these two sites (Figure 5A). As a reasonable approximation, cross-peaks are observed if the ^{13}C-^{13}C distance is less than 6.5 Å, which for Fϕ and Vγ/Vγ' can only occur if pairs of β-sheets are packed together in a face-to-back arrangement [3,4] (taking into account the additional SSNMR structural restraints from Ref. [21]). Strong cross-peaks also correlate the directly bonded amide C O and Cα spins because the MAS rate coincides with the $n = 1$ rotational resonance condition for these spins. Spectra of Med_{1-50} and Med_{30-50} (at MAS rates corresponding to $n = 1$ rotational resonance for Fϕ and Vγ/Vγ') also show cross-peaks correlating the strongly coupled amide C O and Cα spins, but cross-peaks between Fϕ and Vγ/Vγ' are absent (Figure 5B and 5C). Hence for the longer peptides, the Fϕ–Vγ/Vγ' distance is greater than 6.5 , and the molecular packing is thus different in some respect from that of Med_{42-49}. Further structural characterisation of the molecular architecture of Med_{1-50} and Med_{30-50} aggregates was beyond the scope of the present work and materials available at this stage.

Local dynamics within amyloid fibrils have until recently been neglected in structural studies yet potentially carry useful information about the fibril architecture [32–34]. It was investigated whether measurements of site-specific dynamics within the $F^{43}GSV$ region could provide clues about differences in the side chain packing in the three peptide aggregates. The ^{13}C-detected DIPSHIFT SSNMR experiment was used to measure ^{13}C-^{1}H dipolar couplings within the peptide backbone and side chains. Spinning side band patterns extracted from the indirect dimension of the two-dimensional spectrum (e.g., Figure 6A) carry site-specific information about the ^{13}C-^{1}H dipolar anisotropy, which is sensitive

Table 1. Summary of ^{13}C chemical shift values (relative to an external trimethylsilyl propionate (TSP) reference) for the amide carbon (C′), Cα and side chain (β, γ, γ', ϕ) positions of medin peptide aggregates

Res.	Chemical shift (ppm)				
	C′	Cα	Cβ	Cγ(Cγ')[a]	Cϕ[b]
F43	170.4	55.8 (1.5)	35.1 (1.8)	136.9 (2.1)	128.5
	170.3	52.6 (1.6)	39.5 (2.0)	136.0 (2.1)	129.1
	170.6	53.1 (1.6)	38.9 (1.7)	136.0 (2.2)	129.3
G44	169.5	42. 7 (1.3)	—	—	—
	167.9	41.7 (1.4)	—	—	—
	168.2	41.5 (1.5)	—	—	—
S45	171.0	53.6 (2.0)	62.7 (1.0)	—	—
	169.7	52.9 (1.6)	62.9 (1.3)	—	—
	170.2	53.1 (1.6)	62.1 (1.5)	—	—
V46	173.4	58.8 (1.5)	33.6 (1.4)	18.3 (1.2)	—
	172.5	57.7 (1.5)	32.0 (1.4)	18.6 (1.1)	—
	172.9	58.7 (1.6)	32.1 (1.5)	18.5 (1.2)	—

Values for each site correspond to the order (from top to bottom): Med_{42-49}, Med_{30-50}, Med_{1-50}. Where it was possible to measure line widths at half height, values (in ppm) are shown in parentheses.

[a]Chemical shifts for Cγ and Cγ' of Med_{42-49} are equivalent.

[b]Value denotes the midpoint of the chemical shift range.

Journal of PeptideScience

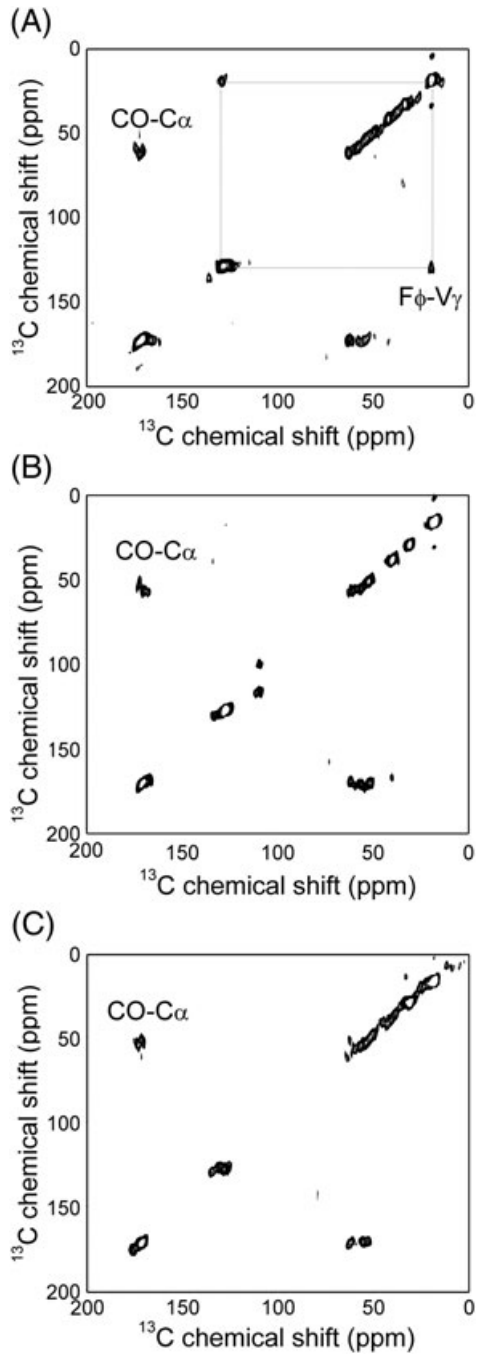

Figure 5. Two-dimensional ^{13}C-^{13}C exchange spectra for Med_{42-49} (A), Med_{30-50} (B) and Med_{1-50} (C). MAS rates correspond to $n = 1$ rotational resonance with respect to the frequencies of Fϕ and Vγ/γ' in each case (11 126, 11 116 and 11 146 Hz, respectively). The Fϕ–Vγ/γ' cross-peak is highlighted by the gray line in (A) but is absent from (B) and (C). In each spectrum, the intensities were normalised between 0 and 1, and peaks are represented by the same 24 contour levels.

to motions on the μs–ms timescale. Increasing motional averaging of the dipolar anisotropy is reflected in a concomitant loss of intensity of the outer side bands and an increase in the centre-band intensity. For each of the peptide aggregates, side band patterns were extracted at the ^{13}C frequencies of the protonated carbon sites. As an example, Figure 6 (B–D) shows the side band patterns for Cϕ of F43 for Med_{42-49}, Med_{30-50} and Med_{1-50} alongside simulated side band patterns calculated for dipolar couplings at the rigid limit. The side band intensities for Med_{42-49} (Figure 6B) are consistent with little or no ring motion on the dipolar timescale, but for Med_{30-50} and Med_{1-50} (Figure 6C and 6D), the side band patterns clearly deviate from the rigid-limit intensities indicating a degree of motional averaging on the μs–ms timescale.

The amplitudes of motion at each site can be expressed as an order parameter *S* [24], which is calculated from the observed coupling strength divided by the rigid-limit coupling. Complete isotropic motional averaging gives an order parameter of zero, and a completely rigid site gives an order parameter of 1. Figure 7 shows values of *S* for the majority of the carbon sites in the three peptide aggregates. For Med_{42-49}, all of the sites have high-order parameters (>0.9), consistent with no motional averaging on the μs–ms timescale of the peptide backbone and side groups, including F43. Residues within amyloid cores tend to be rigid in both the backbone and side chain sites, as observed for prion fibrils [34] and also for stabilised Aβ protofibrils [33], whereas N-terminal and C-terminal flanking residues are more dynamically disordered. It appears that the N-terminal segment of Med_{42-49} is highly ordered and therefore possibly stabilised by a full complement of inter-strand hydrogen bonds and inter-sheet side chain interactions. For Med_{30-50} and Med_{1-50}, the backbone order parameters are also consistent with a rigid amyloid core, but for F43, the order parameters are substantially lower (~0.6) indicating higher amplitudes of motion of the aromatic ring compared with Med_{42-49}. Thus, the dynamics again suggest that the chain packing of Med_{42-49} is rather different from the two longer peptides.

Conclusions

There is an increasing body of detailed structural information on the fibrillar aggregates of β-amyloid, amylin and several other amyloidogenic polypeptides associated with disease, as well as for numerous shorter peptides derived from these molecules. Solid-state NMR has played a key role in providing experimental constraints from which models of fibril architecture have been constructed [11,35,36]. Although medin is the most common form of localised amyloid, virtually nothing is known about its fibrillar assembly at the molecular level. We recently proposed a structural model for the cross-β-spine of Med_{42-49}, but the extent of its relevance to the fibril structure of full-length medin is open to question.

This work shows that full-length medin and the two shorter peptides Med_{30-50} and Med_{42-49} have very different aggregation kinetics culminating in distinct aggregate morphologies, and these differences are reflected in the structure and dynamics of the aggregates at the molecular level. The properties of F43 appear to be particularly diagnostic of differences in the molecular organisation of the Med_{42-49} β-spine compared with Med_{30-50} and Med_{1-50}. In our earlier structural model of the Med_{42-49} β-spine (reproduced from Ref. [21] in Figure 8), F43 and F48 of adjacent β-sheet layers are positioned close enough together to allow a stabilising π-π interaction between them. The fibril architectures of Med_{30-50} and Med_{1-50} may preclude such a π-π interaction because the F43-V46 distance is longer than for Med_{42-49}, and this might explain the higher mobility of F43 ring seen for the two longer peptides. It is also possible that the anomalous chemical shifts seen for F43 of Med_{42-49} (Figure 4B) reflect local distortions in the backbone geometry that are needed to accommodate the π-π interaction.

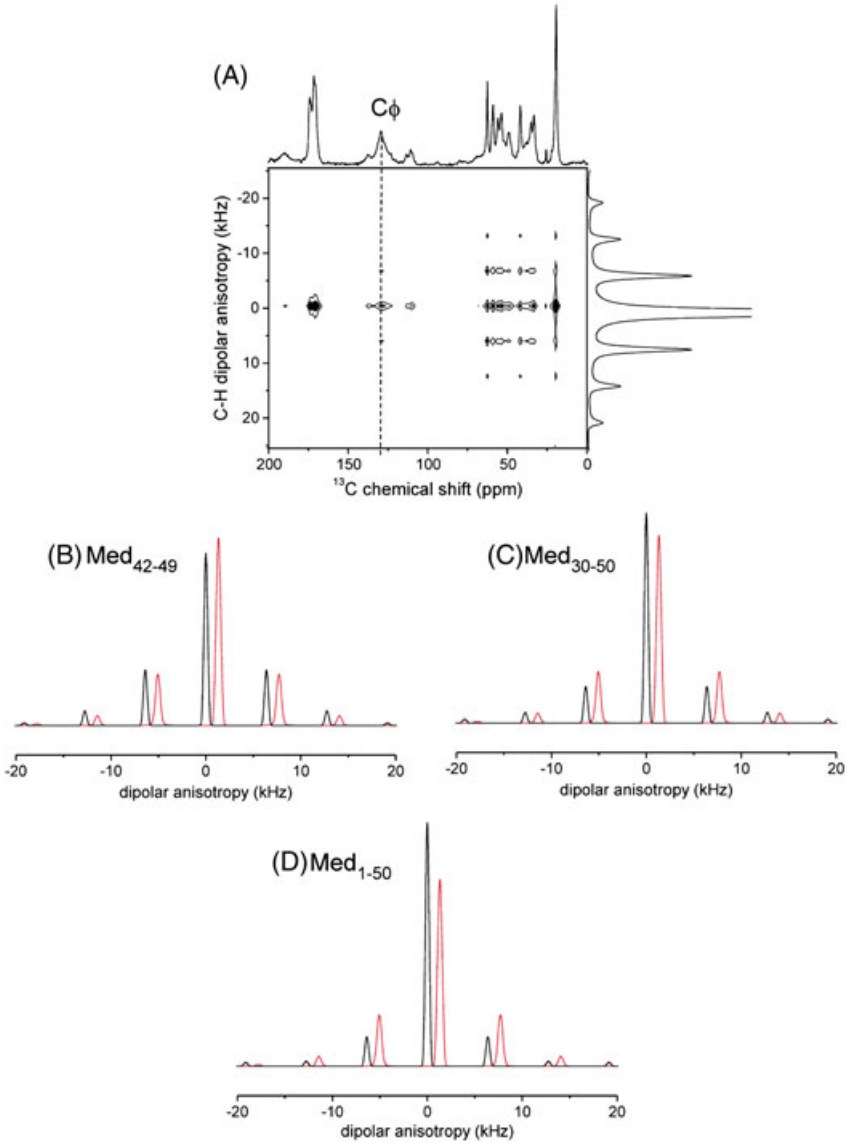

Figure 6. Analysis of the local dynamics within medin peptide aggregates from site-specific measurements of ^{1}H-^{13}C dipolar interactions. (A) An example of a two-dimensional CT-DIPSHIFT spectrum for Med_{42-49}. A corresponding one-dimensional spectrum is shown above the ^{13}C frequency axis at the top, and a slice through the spectrum representing the C-H dipolar anisotropy spectrum at the frequency of Cϕ for F43 (dashed line) is shown along the vertical axis to the right. The dipolar anisotropy spectrum consists of a centre band flanked by a series of side bands separated by the sample spinning frequency. (B–D) Dipolar anisotropy spectra for the F43 aromatic carbons (Fϕ) of Med_{42-49}, Med_{30-50} and Med_{1-50} aggregates. Experimental spectra are shown in black, and simulated rigid-limit dipolar spectra are shown in red.

Until further structural constraints are obtained, it is only possible to speculate on the origins of the different F43 ring position and dynamics for Med_{30-50} and Med_{1-50} compared with Med_{42-49}. Structural models of longer amyloidogenic polypeptides often indicate the presence of one or more turn regions within the fibril structure [35,37–39], whereas fibrils of shorter peptides, including Med_{42-49}, tend to be assembled from linear β-strands [6,21]. The sequence of Med_{1-50} bears similarity to that of the islet amyloid polypeptide amylin, as noted previously [20], and also to the Alzheimer's β amyloid polypeptides $A\beta_{1-40}$ and $A\beta_{1-42}$. Structural models of amylin and $A\beta_{1-40}$ fibrils comprise two extended β-strands separated by a turn [11,38,40]. In the case of $A\beta_{1-40}$, the turn occurs in the region D^{23}VGSNK and is stabilised by a salt bridge between D23 and K28 in the so-called striated ribbon fibril morphology [11]. Given the similarity of this region and the sequence D^{25}LGSSK of medin, it is possible that a similar turn (and Asp-Lys salt bridge) may occur in Med_{1-50} fibrils, which *inter alia* could impose different constraints on the molecular arrangement of the C-terminal residues compared with those observed for Med_{42-49}.

The different aggregate morphologies for Med_{1-50} and Med_{30-50} observed using TEM suggest that truncation of the 19 residues at the N-terminus significantly alters the structure of the fibrils. The similar SSNMR results for Med_{30-50} and Med_{1-50} may therefore not necessarily translate into similar fibril architectures for the two peptides at the molecular level, but further SSNMR measurements are required to confirm this. Taken together, these results imply that at least two of the three predicted amyloidogenic regions are required for the formation and elongation of medin fibres observed in the disease state. These

Journal of PeptideScience

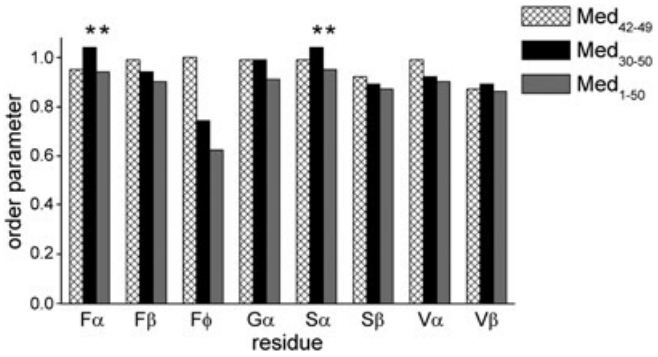

Figure 7. Site-specific order parameters for the medin peptide aggregates. Lower values are consistent with increased amplitudes of motion on the μs–ms timescale. Asterisks indicate that the peaks for Cα of F43 and S45 overlap in the DIPSHIFT spectra, and the values thus represent averages for the two sites.

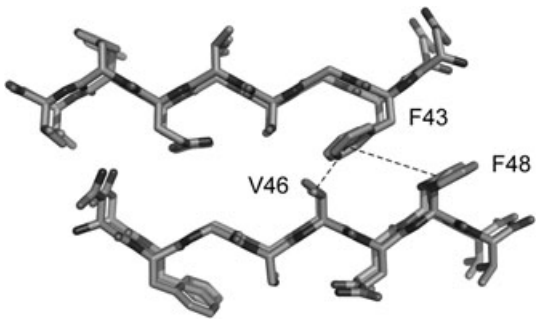

Figure 8. A model of the Med_{42-49} cross-β-spine comprising two β-sheet layers in a face-to-back arrangement [21]. The model satisfies the close through-space distance between F43 and V46 and allows a π-π interaction between F43 and F48 of adjacent β-sheet layers.

results thus provide the motivation for further, more detailed structural studies of this poorly characterised amyloidogenic polypeptide.

References

1 Dobson CM. Protein folding and misfolding. *Nature* 2003; **426**: 884–890.
2 Chiti F, Dobson CM. Protein misfolding, functional amyloid, and human disease. *Annu. Rev. Biochem.* 2006; **75**: 333–366.
3 Nelson R, Sawaya MR, Balbirnie M, Madsen AO, Riekel C, Grothe R, Eisenberg D. Structure of the cross-beta spine of amyloid-like fibrils. *Nature* 2005; **435**: 773–778.
4 Sawaya MR, Sambashivan S, Nelson R, Ivanova MI, Sievers SA, Apostol MI, Thompson MJ, Balbirnie M, Wiltzius JJW, McFarlane HT, Madsen AO, Riekel C, Eisenberg D. Atomic structures of amyloid cross-beta spines reveal varied steric zippers. *Nature* 2007; **447**: 453–457.
5 Tenidis K, Waldner M, Bernhagen J, Fischle W, Bergmann M, Weber M, Merkle ML, Voelter W, Brunner H, Kapurniotu A. Identification of a penta- and hexapeptide of islet amyloid polypeptide (IAPP) with amyloidogenic and cytotoxic properties. *J. Mol. Biol.* 2000; **295**: 1055–1071.
6 Madine J, Jack E, Stockley PG, Radford SE, Serpell LC, Middleton DA. Structural Insights into the polymorphism of amyloid-like fibrils formed by region 20–29 of amylin revealed by solid-state NMR and X-ray fiber diffraction. *J. Am. Chem. Soc.* 2008; **130**: 14990–15001.
7 Amijee H, Madine J, Middleton DA, Doig AJ. Inhibitors of protein aggregation and toxicity. *Biochem. Soc. Trans.* 2009; **37**: 692–696.
8 Tycko R, Sciarretta KL, Orgel JPRO, Meredith SC. Evidence for novel β-sheet structures in Iowa mutant β-amyloid fibrils. *Biochem.* 2009; **48**: 6072–6084.
9 Balbach JJ, Petkova AT, Oyler NA, Antzutkin ON, Gordon DJ, Meredith SC, Tycko R. Supramolecular structure in full-length Alzheimer's beta-amyloid fibrils: evidence for a parallel beta-sheet organization from solid-state nuclear magnetic resonance. *Biophys. J.* 2002; **83**: 1205–1216.
10 Antzutkin ON, Balbach JJ, Leapman RD, Rizzo NW, Reed J, Tycko R. Multiple quantum solid-state NMR indicates a parallel, not antiparallel, organization of β-sheets in Alzheimer's β-amyloid fibrils. *Proc. Natl. Acad. Sci. USA* 2000; **97**: 13045–13050.
11 Petkova AT, Ishii Y, Balbach JJ, Antzutkin ON, Leapman RD, Delaglio F, Tycko R. A structural model for Alzheimer's β-amyloid fibrils based on experimental constraints from solid state NMR. *Proc. Natl. Acad. Sci. USA* 2002; **99**: 16742–16747.
12 Benzinger TLS, Gregory DM, Burkoth TS, Miller-Auer H, Lynn DG, Botto RE, Meredith SC. Two-dimensional structure of beta-amyloid(10–35) fibrils. *Biochemistry* 2000; **39**: 3491–3499.
13 Burkoth TS, Benzinger TLS, Urban V, Morgan DM, Gregory DM, Thiyagarajan P, Botto RE, Meredith SC, Lynn DG. Structure of the β-Amyloid(10–35) Fibril. *J. Am. Chem. Soc.* 2000; **122**: 7883–7889.
14 Balbach JJ, Ishii Y, Antzutkin ON, Leapman RD, Rizzo NW, Dyda F, Reed J, Tycko R. Amyloid fibril formation by A beta(16–22), a seven-residue fragment of the Alzheimer's beta-amyloid peptide, and structural characterization by solid state NMR. *Biochemistry* 2000; **39**: 13748–13759.
15 Petkova AT, Buntkowsky G, Dyda F, Leapman RD, Yau WM, Tycko R. Solid state NMR reveals a pH-dependent antiparallel β-sheet registry in fibrils formed by a β-amyloid peptide. *J. Mol. Biol.* 2004; **335**: 247–260.
16 Mucchiano G, Cornwell GG, Westermark P. Senile aortic amyloid – evidence for 2 distinct forms of localized deposits. *Am. J. Path.* 1992; **140**: 871–877.
17 Peng S, Glennert J, Westermark P. Medin-amyloid: a recently characterized age-associated arterial amyloid form affects mainly arteries in the upper part of the body. *Amyloid* 2005; **12**: 96–102.
18 Peng S, Larsson A, Wassberg E, Gerwins P, Thelin S, Fu X, Westermark P. Role of aggregated medin in the pathogenesis of thoracic aortic aneurysm and dissection. *Lab. Invest.* 2007; **87**: 1195–1205.
19 Larsson A, Söderberg L, Westermark GT, Sletten K, Engström U, Tjernberg LO, Näslund J, Westermark P. Unwinding fibril formation of medin, the peptide of the most common form of human amyloid. *Biochem. Biophys. Res. Commun.* 2007; **361**: 822–828.
20 Reches M, Gazit E. Amyloidogenic hexapeptide fragment of medin: homology to functional islet amyloid polypeptide fragments. *Amyloid* 2004; **11**: 81–89.
21 Madine J, Copland A, Serpell LC, Middleton DA. Cross-beta spine architecture of fibrils formed by the amyloidogenic segment NFGSVQFV of medin from solid-state NMR and X-ray fiber diffraction measurements. *Biochemistry* 2009; **48**: 3089–3099.
22 Bennett AE, Rienstra CM, Auger M, Lakshmi KV, Griffin RG. Heteronuclear decoupling in rotating solids. *J. Chem. Phys.* 1995; **103**: 6951–6958.
23 Takegoshi K, Nakamura S, Terao T. C-13-H-1 dipolar-assisted rotational resonance in magic-angle spinning NMR. *Chem. Phys. Lett.* 2001; **344**: 631–637.
24 Huster D, Xiao LS, Hong M. Solid-state NMR investigation of the dynamics of the soluble and membrane-bound colicin Ia channel-forming domain. *Biochemistry* 2001; **40**: 7662–7674.
25 Boland MP, Middleton DA. The dynamics and orientation of a lipophilic drug within model membranes determined by C-13 solid-state NMR. *Phys. Chem. Chem. Phys.* 2008; **10**: 178–185.
26 Tartaglia GG, Pawar AP, Campioni S, Dobson CM, Chiti F, Vendruscolo M. Prediction of aggregation-prone regions in structured proteins. *J. Mol. Biol.* 2008; **380**: 425–436.
27 Conchillo-Solé O, de Groot NS, Avilés FX, Vendrell J, Daura X, Ventura S. AGGRESCAN: a server for the prediction and evaluation of "hot spots" of aggregation in polypeptides. *BMC Bioinforma.* 2007; **8**: 65–82.
28 Trovato A, Seno F, Tosatto SCE. The PASTA server for protein aggregation prediction. *Protein Eng. Des. Sel.* 2007; **20**: 521–523.
29 Groenning M. Binding mode of thioflavin T and other molecular probes in the context of amyloid fibrils – current status. *J. Chem. Biol.* 2010; **3**: 1–18.
30 Krebs MRH, Bromley EHC, Donald AM. The binding of thioflavin-T to amyloid fibrils: localisation and implications. *J. Struct. Biol.* 2005; **149**: 30–37.
31 Mao XB, Guo YY, Wang CX, Zhang M, Ma XJ, Liu L, Niu L, Zeng QD, Yang YL, Wang C. Binding modes of thioflavin T molecules to prion peptide assemblies identified by using scanning tunneling microscopy. *ACS Chem. Neurosci.* 2011; **2**: 281–287.
32 Sackewitz M, Scheidt HA, Lodderstedt G, Schierhorn A, Schwarz E, Huster D. Structural and dynamical characterization of fibrils from a

disease-associated alanine expansion domain using proteolysis and solid-state NMR spectroscopy. *J. Am. Chem. Soc.* 2008; **130**: 7172–7173.
33 Scheidt HA, Morgado I, Rothemund S, Huster D, Fandrich M. Solid-State NMR spectroscopic investigation of A beta protofibrils: implication of a beta-sheet remodeling upon maturation into terminal amyloid fibrils. *Angew. Chem. Int. Ed.* 2011; **50**: 2837–2840.
34 Helmus JJ, Surewicz K, Surewicz WK, Jaroniec CP. Conformational flexibility of Y145Stop human prion protein amyloid fibrils probed by solid-state nuclear magnetic resonance spectroscopy. *J. Am. Chem. Soc.* 2010; **132**: 2393–2403.
35 Iwata K, Fujiwara T, Matsuki Y, Akutsu H, Takahashi S, Naiki H, Goto Y. 3D structure of amyloid protofilaments of β2-microglobulin fragment probed by solid-state NMR. *Proc. Natl. Acad. Sci. USA* 2006; **103**: 18119–18124.
36 Jaroniec CP, MacPhee CE, Bajaj VS, McMahon MT, Dobson CM, Griffin RG. High-resolution molecular structure of a peptide in an amyloid fibril determined by magic angle spinning NMR spectroscopy. *Proc. Natl. Acad. Sci. USA* 2004; **101**: 711–716.
37 Tycko R. Progress towards a molecular-level structural understanding of amyloid fibrils. *Curr. Opin. Struct. Biol.* 2004; **14**: 96–103.
38 Luca S, Yau WM, Leapman R, Tycko R. Peptide conformation and supramolecular organization in amylin fibrils: constraints from solid-state NMR. *Biochem.* 2007; **46**: 13505–13522.
39 Wasmer C, Lange A, Van Melckebeke H, Siemer AB, Riek R, Meier BH. Amyloid fibrils of the HET-s(218–289) prion form a β solenoid with a triangular hydrophobic core. *Science* 2008; **319**: 1523–1526.
40 Paravastu AK, Leapman RD, Yau WM, Tycko R. Molecular structural basis for polymorphism in Alzheimer's β-amyloid fibrils. *Proc. Natl. Acad. Sci. USA* 2008; **105**: 18349–18354.
41 Wang Y, Jardetzky O. Probability-based protein secondary structure identification using combined NMR chemical-shift data. *Protein Sci.* 2002; **11**: 852–861.

